

(ACC), Precision (PRE), Recall (REC), and F1 Score (F1). Fig. 3 presents the overall experimental results in the form of violin plots, where each subplot displays outcomes based on the aggregate dataset and the three disease-specific datasets. Each point within the plots represents an experimental pair of patient samples, providing a detailed visual representation of the model's performance across various conditions.

Overall, the model achieved an average accuracy of 84.83%, with precision at 86.23%, recall at 81.51%, and an F1 score of 80.92% across all datasets, indicating robust predictive capabilities. In assessing the scGSL model across three distinctive datasets, each showed varied but generally effective performance metrics. The Leukemia dataset showed a robust average accuracy of 86.85% and precision at 78.46%, though it had slightly lower recall and F1 scores at 75.23% and 73.39%, respectively. The Breast Invasive Carcinoma dataset maintained a balanced performance with an average accuracy of 83.56% and a notably high precision of 89.42%. In the Colorectal Cancer dataset, the model excelled with an average accuracy of 86.52%, complemented by consistent precision and recall rates of 86.44% and 86.07%. These findings across the datasets underline the scGSL model's robust predictive capabilities and highlight its potential applicability in diverse clinical scenarios.

sc5rJUQ060-sc5rJUQ033	71.26	71.52	52.34	41.53	74.77	70.92	79.55	44.26	72.51	66.50	<u>75.21</u>
sc5rJUQ050-sc5rJUQ060	69.77	<u>76.15</u>	64.48	25.38	74.81	69.90	72.64	60.40	62.21	64.45	76.34
sc5rJUQ060-sc5rJUQ050	86.75	<u>93.67</u>	51.33	47.75	85.32	88.44	60.30	84.63	87.87	76.97	94.67
GSM4555888-GSM4555891	84.35	91.96	72.09	68.04	85.69	72.40	73.97	85.45	62.47	84.82	<u>87.12</u>
GSM4555891-GSM4555888	90.15	82.36	87.13	29.19	89.41	89.31	63.50	83.23	<u>90.41</u>	89.41	90.57
Average	71.39	<u>78.94</u>	62.37	38.99	77.39	70.11	65.29	62.08	70.18	63.89	82.14

Table 3. Comparative Performance of Different Models on the Colorectal Cancer Dataset (Best Performance in Bold, Second Best Underlined).

Experiment	Seurat	Single R	CHET AH	scmap Cell	singleCellNet	scLearn	scPred	Marker Count	scClassify	sciBet	Ours
scrEXT009-scrEXT010	76.45	85.20	79.12	54.36	<u>89.04</u>	84.13	64.81	76.39	87.10	85.66	89.61
scrEXT010-scrEXT009	66.43	83.95	76.93	40.11	79.11	<u>87.50</u>	75.58	84.88	84.97	81.21	88.35
scrEXT009-scrEXT020	62.14	<u>90.03</u>	55.85	49.50	73.95	85.46	26.47	69.38	78.16	85.99	90.45
scrEXT020-scrEXT009	71.48	<u>77.57</u>	72.69	29.87	70.13	73.26	77.78	68.44	70.55	73.02	74.53
scrEXT010-scrEXT020	82.08	<u>92.52</u>	67.77	57.86	82.38	89.97	90.68	75.07	91.04	89.97	93.89
scrEXT020-scrEXT010	70.77	64.07	80.94	32.28	80.56	81.23	86.41	75.32	80.51	82.21	<u>82.32</u>
Average	71.56	82.22	72.22	44.00	79.19	<u>83.59</u>	70.29	74.92	82.06	83.01	86.52

Fig. 4 Comparison of Cell Embeddings and Raw Data Distributions between scGSL and Other Methods.

3.3 Ablation Study for scGSL with Different Settings

In constructing the cell-cell graph for the scGSL model, HVGs are first selected, followed by the application of the KNN algorithm to establish an initial graph structure. Given that scGSL is a model based on GNN, this section systematically examines the impact of both the selection of the KNN algorithm and the HVG filtering criteria on the predictive performance of scGSL.

For the former, Fig. 5a displays violin scatter plots comparing the scGSL model's performance across different datasets under various KNN settings. The standard setting of K=0.2% total cell count and embedding size of 128 (K=0.2%, ES=128) consistently delivered superior results, achieving the highest average accuracy and F1-score. Other tested settings included K=0.1% & ES=128, K=0.5% & ES=128, K=0.2% & ES=64, and K=0.2% & ES=256. None of these configurations could match the ACC and F1 results of the standard setting. This emphasizes the effectiveness and robustness of the K=0.2% and ES=128 configuration in the scGSL model for optimal cell type classification performance.

To compare different gene selection strategies, we collated gene sets from six gene signaling pathway databases, including KEGG and Reactome, as well as the cell state marker gene database (CancerSEA database) and the LRI database [19, 35-39]. We used the genes found within each of these individual databases as criteria for gene selection, which were then used to construct node features in our graph-based model. Fig. 5b showcases a heatmap of the scGSL model's performance, combining these varied selection approaches on the E-MTAB-8107 dataset, which includes data from 10 pairs of patients across five distinct patients. In our comparative analysis of gene selection strategies across several databases, our method (HVG3000) demonstrated superior performance with an ACC of 81.47%, PRE of 88.39%, REC of 82.49%, and F1 of 82.58%. Fig. 5c illustrates a comparison of cell type prediction accuracies in the GSE132509 dataset, using the scGSL model both with and without the GSL component. The results demonstrate that the inclusion of GSL significantly enhances predictive accuracy. Specifically, the average accuracy with GSL was 90.89%, compared to 87.55% when GSL was not utilized. This improvement underscores the effectiveness of GSL in enhancing the precision

validated gene pairs, we assess the statistical significance of these interactions in the constructed cell-cell graphs (visualized in Fig. 6). In the Leukemia dataset, the "SPRY1-LAT" and "BSG-ATP2B4" gene pairs within CD8T cells are investigated, confirmed by studies referenced in PMID19915061 [40] and PMID26729804 [41]; in the Breast Invasive Carcinoma dataset, the "ATP2A3-SP1" and "ZAP70-TLN1" gene pairs within CD8T cells are investigated, as established in the literature with PMIDs 22851172 [42] and 20488542 [43]; in the Colorectal Cancer dataset, the "BIRC5-CASP6" and "PSMC3-SIRT7" gene pairs within malignant cells are investigated, documented in PMIDs 23856250 [44] and 28435470 [45].

Specifically, we focused on the above particular gene pairs within a certain cell type, such as the CD8T cell subgraph in the Leukemia Dataset. We categorized the cells into two groups: one containing cells connected by an edge and the other consisting of cells without an edge, which served as the background group. We then conducted the Mann-Whitney U test to compare the expression levels of the two genes in the gene pair between these groups. If the p-value from this test is less than 0.05, it indicates that the differences in gene expression are statistically significant. Such a significant result would support the claim that the gene pair's expression differences, as learned by the scGSL from the cell-cell graph, are biologically meaningful.

It is noted that the generation of the cell-cell graphs was generated in an unsupervised manner, meaning that the gene pairs validated were not involved in the model training process. As a result, Tables 4, 5, and 6 present findings from three different cancer datasets: Leukemia, Breast Invasive Carcinoma, and Colorectal Cancer. In the Leukemia dataset, the gene pair "SPRY1-LAT" achieved significant p-values (less than 0.05) in 7 out of 12 experiments, while "BSG-

ATP2B4" showed significance in 10 out of 12 experiments. In the dataset for Breast Invasive Carcinoma, every experiment involving the gene pair "ATP2A3-SP1" resulted in significant p-values, and "ZAP70-TLN1" was significant in 6 out of 8 experiments. In the Colorectal Cancer dataset, "BIRC5-CASP6" was significant in 7 out of 8 experiments, and "PSMC3-SIRT7" in 6 out of 8. These results underscore the robustness and biological relevance of the unsupervised cell-cell graph approach, as it successfully identified biologically meaningful gene interactions across various types of cancer without prior knowledge of these interactions during the model's training phase.

Table 4. Statistical Significance of Known Gene Interactions for CD8+ T Cells in Constructed Cell-Cell Graphs on the Leukemia Dataset (P-Value < 0.05 Highlighted).

Experiment	SPRY1	LAT	BSG	ATP2B4
PBMMC_1-2	<u>1.67403e-04</u>	<u>9.46e-27</u>	<u>7.01e-33</u>	<u>7.92883e-04</u>
PBMMC_2-1	1.15814e-01	3.42939e-01	<u>3.92324e-03</u>	<u>2.50337e-02</u>
PBMMC_1-3	<u>1.53503e-03</u>	<u>8.07e-05</u>	<u>6.01e-05</u>	<u>7.62435e-03</u>
PBMMC_3-1	1.22120e-01	1.46373e-01	<u>3.58655e-02</u>	<u>9.62522e-03</u>
PBMMC_2-3	<u>4.06214e-03</u>	<u>4.93204e-03</u>	<u>1.51e-06</u>	<u>1.42773e-02</u>
PBMMC_3-2	3.44669e-01	<u>5.62577e-03</u>	3.48405e-01	1.68556e-01

Table 5. Statistical Significance of Known Gene Interactions for CD8+ T Cells in Constructed Cell-Cell Graphs on the Breast Invasive Carcinoma Dataset (P-Value < 0.05 Highlighted).

Experiment	ATP2A3	SP1	ZAP70	TLN1
sc5rJUQ024-26	<u>1.29373e-04</u>	<u>1.27737e-04</u>	1.17708e-01	<u>3.21875e-02</u>
sc5rJUQ026-24	<u>2.18143e-02</u>	<u>6.93e-09</u>	1.76564e-01	<u>4.67e-27</u>
sc5rJUQ024-33	<u>1.29e-12</u>	<u>1.04e-07</u>	<u>7.00e-07</u>	<u>8.78e-16</u>
sc5rJUQ033-24	<u>1.77e-13</u>	<u>2.57e-15</u>	<u>8.95e-07</u>	<u>4.98e-21</u>

Table 6. Statistical Significance of Known Gene Interactions for Malignant Cells in Constructed Cell-Cell Graphs on the Colorectal Cancer Dataset (P-Value < 0.05 Highlighted).

Experiment	BIRC5	CASP6	PSMC3	SIRT7
scrEXT009-10	<u>2.41032e-02</u>	<u>7.15088e-03</u>	<u>9.11823e-03</u>	4.93301e-01
scrEXT010-09	<u>4.35e-16</u>	<u>1.11573e-03</u>	<u>1.16e-12</u>	<u>1.68677e-02</u>
scrEXT009-20	<u>1.19508e-02</u>	3.99906e-01	<u>3.38843e-01</u>	9.50344e-02
scrEXT020-09	<u>6.53e-15</u>	<u>1.97e-05</u>	<u>6.16e-15</u>	<u>7.71e-06</u>

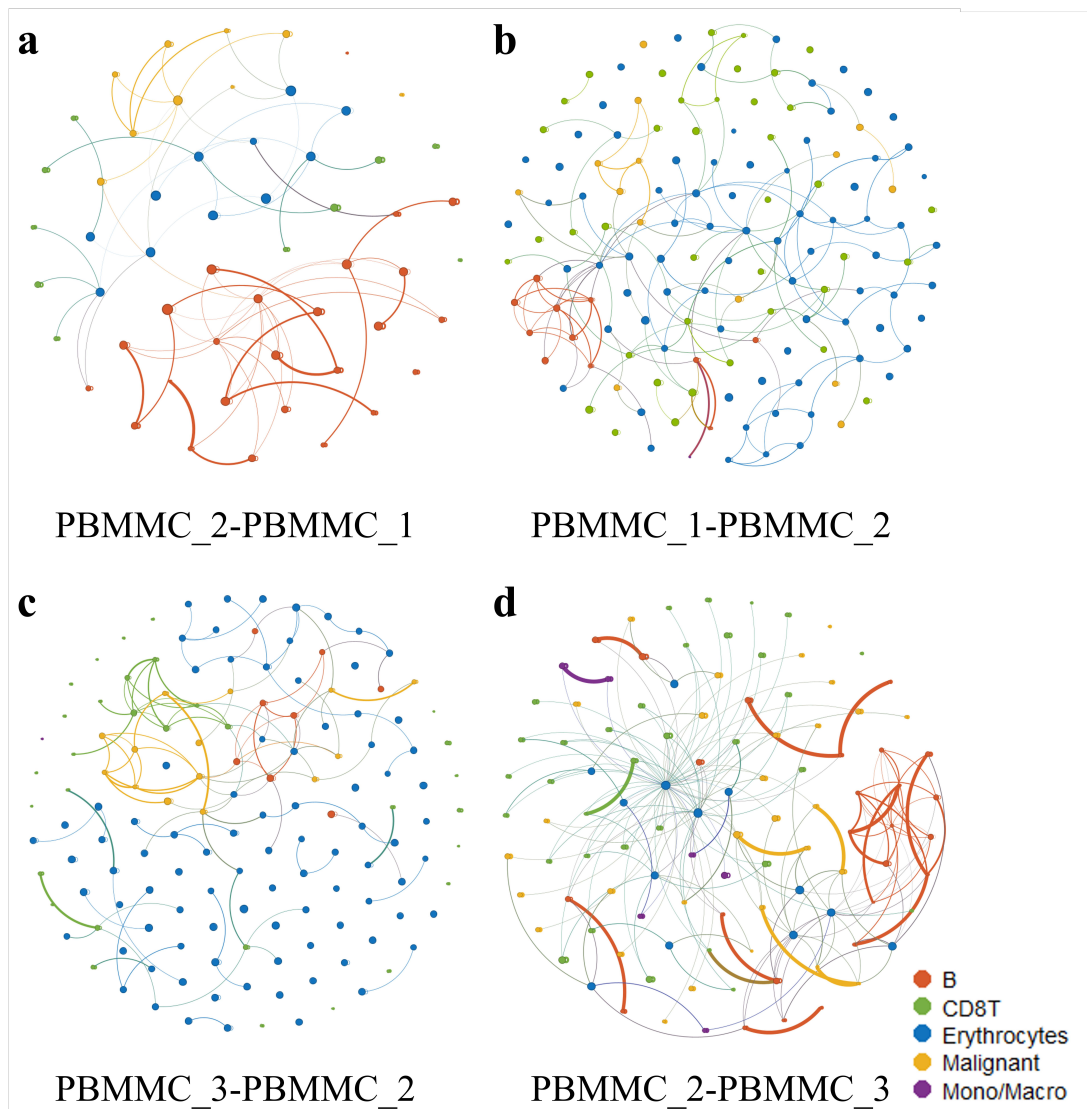


Fig. 6 Visualization of Cell-Cell Graphs Derived from scGSL on the Leukemia Dataset.

4 Conclusions

The scGSL model represents a significant advancement in the analysis of non-spatial transcriptomic scRNA-seq data within the context of cancer research. By leveraging GNN and graph domain adaptation, our model not only enhances the accuracy of cell type annotation but also provides a deeper understanding of the intricate cellular interactions within the TME. The ability of the scGSL model to autonomously generate and refine cell-cell interaction graphs based on intrinsic labels ensures a more biologically accurate representation of intercellular

communication. This is crucial for identifying potential therapeutic targets and understanding the complex network of interactions that drive tumor progression and resistance to therapies.

Despite its robust performance, the scGSL model faces certain challenges and limitations. One significant challenge is the inherent complexity of TMEs, which can vary widely between different types of cancers and even between patients with the same type of cancer. This variability can affect the generalizability of the model across different datasets and cancer types. Additionally, the reliance on labeled data from specific cancer types for training may limit the model's applicability to cancers with less available data. Furthermore, the model's performance is contingent on the quality and completeness of the underlying scRNA-seq data, which can be affected by technical variations and sampling errors.

5 Funding

This research was funded by the National Science Fund for Distinguished Young Scholars of China under grant number: 62325308; the Science and Technology Innovation 2030–New Generation Artificial Intelligence Major Project under grant number No. 2018AAA0100103; the National Natural Science Foundation of China under grant number 62002297, grant number 61722212, grant number 62072378, grant number 62273284, grant number 62472353, grant number 62302495, and grant number 62172338; the Neural Science Foundation of Shaanxi Province under grant number: 2022JQ-700; the Fundamental Research Funds for the Central Universities under grant number: D5000230199; the Guangdong Basic and Applied Basic Research Foundation under grant number 2024A1515011984; and the Fundamental Research

Funds for the Central Universities under grant number G2023KY05102.

6 Declaration of competing interest

The authors declare that they have no conflicts of interest in this work.

Reference

- [1] L. Peng *et al.*, "Cell–cell communication inference and analysis in the tumour microenvironments from single-cell transcriptomics: data resources and computational strategies," *Briefings in bioinformatics*, vol. 23, no. 4, p. bbac234, 2022.
- [2] H. Choi *et al.*, "Transcriptome analysis of individual stromal cell populations identifies stroma-tumor crosstalk in mouse lung cancer model," *Cell reports*, vol. 10, no. 7, pp. 1187-1201, 2015.
- [3] R. Browaeys, W. Saelens, and Y. Saeys, "NicheNet: modeling intercellular communication by linking ligands to target genes," *Nature methods*, vol. 17, no. 2, pp. 159-162, 2020.
- [4] S. R. Tyler *et al.*, "PyMINER finds gene and autocrine-paracrine networks from human islet scRNA-Seq," *Cell reports*, vol. 26, no. 7, pp. 1951-1964. e8, 2019.
- [5] S. Wang, M. Karikomi, A. L. MacLean, and Q. Nie, "Cell lineage and communication network inference via optimization for single-cell transcriptomics," *Nucleic acids research*, vol. 47, no. 11, pp. e66-e66, 2019.
- [6] S. Cabello-Aguilar, M. Alame, F. Kon-Sun-Tack, C. Fau, M. Lacroix, and J. Colinge, "SingleCellSignalR: inference of intercellular networks from single-cell transcriptomics," *Nucleic acids research*, vol. 48, no. 10, pp. e55-e55, 2020.
- [7] A. R. Cillo *et al.*, "Immune landscape of viral-and carcinogen-driven head and neck cancer," *Immunity*, vol. 52, no. 1, pp. 183-199. e9, 2020.
- [8] Z. Cang and Q. Nie, "Inferring spatial and signaling relationships between cells from single cell transcriptomic data," *Nature communications*, vol. 11, no. 1, p. 2084, 2020.
- [9] D. Schapiro *et al.*, "histoCAT: analysis of cell phenotypes and interactions in multiplex image cytometry data," *Nature methods*, vol. 14, no. 9, pp. 873-876, 2017.
- [10] X. Cao *et al.*, "scPriorGraph: constructing biosemantic cell–cell graphs with prior gene set selection for cell type identification from scRNA-seq data," *Genome Biology*, vol. 25, no. 1, p. 207, 2024.
- [11] T. Stuart *et al.*, "Comprehensive integration of single-cell data," *cell*, vol. 177, no. 7, pp. 1888-1902. e21, 2019.
- [12] D. Aran *et al.*, "Reference-based analysis of lung single-cell sequencing reveals a transitional profibrotic macrophage," *Nature immunology*, vol. 20, no. 2, pp. 163-172,

- 2019.
- [13] A. W. Zhang *et al.*, "Probabilistic cell-type assignment of single-cell RNA-seq for tumor microenvironment profiling," *Nature methods*, vol. 16, no. 10, pp. 1007-1015, 2019.
 - [14] X. Shao, J. Liao, X. Lu, R. Xue, N. Ai, and X. Fan, "scCATCH: automatic annotation on cell types of clusters from single-cell RNA sequencing data," *Iscience*, vol. 23, no. 3, 2020.
 - [15] Q. Song, J. Su, and W. Zhang, "scGCN is a graph convolutional networks algorithm for knowledge transfer in single cell omics," *Nature communications*, vol. 12, no. 1, p. 3826, 2021.
 - [16] S. Jin *et al.*, "Inference and analysis of cell-cell communication using CellChat," *Nature communications*, vol. 12, no. 1, p. 1088, 2021.
 - [17] Z.-H. Du *et al.*, "scPML: pathway-based multi-view learning for cell type annotation from single-cell RNA-seq data," *Communications Biology*, vol. 6, no. 1, p. 1268, 2023.
 - [18] S. Aibar *et al.*, "SCENIC: single-cell regulatory network inference and clustering," *Nature methods*, vol. 14, no. 11, pp. 1083-1086, 2017.
 - [19] M. Kanehisa and S. Goto, "KEGG: kyoto encyclopedia of genes and genomes," *Nucleic acids research*, vol. 28, no. 1, pp. 27-30, 2000.
 - [20] C. Di Genua *et al.*, "C/EBP α and GATA-2 mutations induce bilineage acute erythroid leukemia through transformation of a neomorphic neutrophil-erythroid progenitor," *Cancer Cell*, vol. 37, no. 5, pp. 690-704. e8, 2020.
 - [21] M. Caron *et al.*, "Single-cell analysis of childhood leukemia reveals a link between developmental states and ribosomal protein expression as a source of intra-individual heterogeneity," *Scientific reports*, vol. 10, no. 1, p. 8079, 2020.
 - [22] J. K. Bailur *et al.*, "Risk-associated alterations in marrow T cells in pediatric leukemia," *JCI insight*, vol. 5, no. 16, 2020.
 - [23] J. Qian *et al.*, "A pan-cancer blueprint of the heterogeneous tumor microenvironment revealed by single-cell profiling," *Cell research*, vol. 30, no. 9, pp. 745-762, 2020.
 - [24] Y. Chi *et al.*, "Cancer cells deploy lipocalin-2 to collect limiting iron in leptomeningeal metastasis," *Science*, vol. 369, no. 6501, pp. 276-282, 2020.
 - [25] S. Liu, D. Zou, H. Zhao, and P. Li, "Pairwise Alignment Improves Graph Domain Adaptation," *arXiv preprint arXiv:2403.01092*, 2024.
 - [26] E. Candes and B. Recht, "Exact matrix completion via convex optimization," *Communications of the ACM*, vol. 55, no. 6, pp. 111-119, 2012.
 - [27] H. Kim, J. Lee, K. Kang, and S. Yoon, "MarkerCount: A stable, count-based cell type identifier for single-cell RNA-seq experiments," *Computational and Structural Biotechnology Journal*, vol. 20, pp. 3120-3132, 2022.
 - [28] J. K. De Kanter, P. Lijnzaad, T. Candelli, T. Margaritis, and F. C. Holstge, "CHETAH: a selective, hierarchical cell type identification method for single-cell RNA sequencing," *Nucleic acids research*, vol. 47, no. 16, pp. e95-e95, 2019.
 - [29] Y. Tan and P. Cahan, "SingleCellNet: a computational tool to classify single cell RNA-Seq data across platforms and across species," *Cell systems*, vol. 9, no. 2, pp. 207-213. e2, 2019.

- [30] B. Duan *et al.*, "Learning for single-cell assignment," *Science advances*, vol. 6, no. 44, p. eabd0855, 2020.
- [31] J. Alquicira-Hernandez, A. Sathe, H. P. Ji, Q. Nguyen, and J. E. Powell, "scPred: accurate supervised method for cell-type classification from single-cell RNA-seq data," *Genome biology*, vol. 20, pp. 1-17, 2019.
- [32] V. Y. Kiselev, A. Yiu, and M. Hemberg, "scmap: projection of single-cell RNA-seq data across data sets," *Nature methods*, vol. 15, no. 5, pp. 359-362, 2018.
- [33] C. Li *et al.*, "SciBet as a portable and fast single cell type identifier," *Nature communications*, vol. 11, no. 1, p. 1818, 2020.
- [34] Y. Lin *et al.*, "scClassify: sample size estimation and multiscale classification of cells using single and multiple reference," *Molecular systems biology*, vol. 16, no. 6, p. e9389, 2020.
- [35] M. Gillespie *et al.*, "The reactome pathway knowledgebase 2022," *Nucleic acids research*, vol. 50, no. D1, pp. D687-D692, 2022.
- [36] M. Martens *et al.*, "WikiPathways: connecting communities," *Nucleic acids research*, vol. 49, no. D1, pp. D613-D621, 2021.
- [37] E. G. Cerami *et al.*, "Pathway Commons, a web resource for biological pathway data," *Nucleic acids research*, vol. 39, no. suppl_1, pp. D685-D690, 2010.
- [38] H. Yuan *et al.*, "CancerSEA: a cancer single-cell state atlas," *Nucleic acids research*, vol. 47, no. D1, pp. D900-D908, 2019.
- [39] Y. Yuan and Z. Bar-Joseph, "GCNG: graph convolutional networks for inferring gene interaction from spatial transcriptomics data," *Genome biology*, vol. 21, pp. 1-16, 2020.
- [40] J. S. Lee *et al.*, "Recruitment of Sprouty1 to immune synapse regulates T cell receptor signaling," *The Journal of Immunology*, vol. 183, no. 11, pp. 7178-7186, 2009.
- [41] V. Supper *et al.*, "Association of CD147 and calcium exporter PMCA4 uncouples IL-2 expression from early TCR signaling," *The Journal of Immunology*, vol. 196, no. 3, pp. 1387-1399, 2016.
- [42] S. Ghosh *et al.*, "Nifetepimine, a dihydropyrimidone, ensures CD4+ T cell survival in a tumor microenvironment by maneuvering sarco (endo) plasmic reticulum Ca²⁺ ATPase (SERCA)," *Journal of Biological Chemistry*, vol. 287, no. 39, pp. 32881-32896, 2012.
- [43] Y.-P. Lin, Y.-J. Cheng, J.-Y. Huang, H.-C. Lin, and B.-C. Yang, "Zap70 controls the interaction of talin with integrin to regulate the chemotactic directionality of T-cell migration," *Molecular immunology*, vol. 47, no. 11-12, pp. 2022-2029, 2010.
- [44] F. Végran *et al.*, "Survivin-3B potentiates immune escape in cancer but also inhibits the toxicity of cancer chemotherapy," *Cancer research*, vol. 73, no. 17, pp. 5391-5401, 2013.
- [45] M. Tang *et al.*, "Downregulation of SIRT7 by 5-fluorouracil induces radiosensitivity in human colorectal cancer," *Theranostics*, vol. 7, no. 5, p. 1346, 2017.

Supplementary File 1

Updating θ . To update θ , we fix S and eliminate terms that do not pertain to θ . Consequently, the objective function in Equation (5) simplifies to $\mathcal{L}_{cls}(\theta, A, X, Y)$, which we can simply learn θ via stochastic gradient descent.

Updating S . To update S , we fix θ and eliminate terms that do not pertain to S . Consequently, the objective function in Equation (5) simplifies to:

$$\min_S \mathcal{L}(S, A) + \alpha \|S\|_1 + \beta \|S\|_* \quad s.t., S = S^T \quad (1)$$

where $\mathcal{L}(S, A) = \|A - S\|_F^2 + \gamma \mathcal{L}_{cls} + \lambda \mathcal{L}_{graph}$ (2)

It should be noted that both the ℓ_1 norm and the nuclear norm are inherently non-differentiable. In scenarios where the optimization problem incorporates a singular non-differentiable regularizer $R(S)$, the application of Forward-Backward splitting methods [1] is advisable. This approach alternates between a gradient descent step and a proximal step, as described below:

$$S^{(k)} = \text{prox}_{\eta R} \left(S^{(k-1)} - \eta \nabla_S \mathcal{L}(S, A) \right), \quad (2)$$

where η represents the learning rate, and $\text{prox}R$ denotes the proximal operator, defined as follow:

$$\text{prox}_R(Z) = \arg \min_S \frac{1}{2} \|S - Z\|_F^2 + R(S) \quad (3)$$

Specifically, the proximal operators for the ℓ_1 norm and the nuclear norm can be expressed as:

$$\text{prox}_{\alpha \|\cdot\|_1}(Z) = \text{sgn}(Z) \odot (|Z| - \alpha)_+ \quad , \quad (4)$$

$$\text{prox}_{\beta \|\cdot\|_*}(Z) = \text{Udiag}((\sigma_i - \beta)_+) V^T \quad , \quad (5)$$

where $Z = \text{Udiag}(\sigma_1, \dots, \sigma_n) V^T$ is the singular value decomposition of Z . To manage the optimization of an objective function that includes two non-differentiable regularizers, Richard et al. [2] propose the Incremental Proximal Descent method, utilizing the aforementioned proximal operators. This method involves cyclically iterating the update process, allowing for the updating of S as described below:

$$\begin{cases} S^{(k)} = S^{(k-1)} - \eta \cdot \nabla_S (\mathcal{L}(S, A)), \\ S^{(k)} = \text{prox}_{\eta \beta \|\cdot\|_*}(S^{(k)}), \\ S^{(k)} = \text{prox}_{\eta \alpha \|\cdot\|_1}(S^{(k)}), \end{cases} \quad (6)$$

Once we have learned a relaxed version of S , we project it to satisfy specific constraints. For the symmetry constraint, we define S as $S=(S+S^T)/2$. Regarding the constraint that each element S_{ij} must lie within the range $[0, 1]$, we project any S_{ij} values less than 0 to 0 and any greater than 1 to 1. We denote these projection procedures as $P_S(S)$.

Training Algorithm:

Initialize $S \leftarrow A$

Randomize θ

while the error has not converged **do**

$$S \leftarrow S - \eta \cdot \nabla_S (\|A - S\|_F^2 + \gamma \mathcal{L}_{cls} + \lambda \mathcal{L}_{graph})$$

$$S \leftarrow \text{prox}_{\eta\beta\|\cdot\|_*}(S)$$

$$S \leftarrow \text{prox}_{\eta\alpha\|\cdot\|_1}(S)$$

$$S \leftarrow P_S(S)$$

for $i = 1$ to τ **do**

$$g \leftarrow \frac{\partial \mathcal{L}_{cls}(\theta, A, X, Y)}{\partial \theta}$$

$$\theta \leftarrow \theta - \eta' g$$

Return S, θ

Reference

[1] Combettes, Patrick L., and Jean-Christophe Pesquet. "Proximal splitting methods in signal processing." *Fixed-point algorithms for inverse problems in science and engineering* (2011): 185-212.

[2] Raguet, Hugo, Jalal Fadili, and Gabriel Peyré. "A generalized forward-backward splitting." *SIAM Journal on Imaging Sciences* 6.3 (2013): 1199-1226.